Population of sensory neurons essential for asthmatic hyperreactivity of inflamed airways

Dimitri Tränkner[a], Nadeau Hahne[a], Ken Sugino[a], Mark A. Hoon[b], and Charles Zuker[a,c,d,e,1]

[a]Janelia Farm Research Campus, Howard Hughes Medical Institute, Ashburn, VA 20147; [b]National Institute of Dental and Craniofacial Research, National Institutes of Health, Bethesda, MD 20892; and [c]Department of Biochemistry and Molecular Biophysics, [d]Department of Neuroscience, and [e]Howard Hughes Medical Institute, Columbia College of Physicians and Surgeons, Columbia University, NY 10032

Contributed by Charles Zuker, June 25, 2014 (sent for review April 30, 2014; reviewed by Dan Littman)

Asthma is a common debilitating inflammatory lung disease affecting over 200 million people worldwide. Here, we investigated neurogenic components involved in asthmatic-like attacks using the ovalbumin-sensitized murine model of the disease, and identified a specific population of neurons that are required for airway hyperreactivity. We show that ablating or genetically silencing these neurons abolished the hyperreactive broncho-constrictions, even in the presence of a fully developed lung inflammatory immune response. These neurons are found in the vagal ganglia and are characterized by the expression of the transient receptor potential vanilloid 1 (TRPV1) ion channel. However, the TRPV1 channel itself is not required for the asthmatic-like hyperreactive airway response. We also demonstrate that optogenetic stimulation of this population of TRP-expressing cells with channelrhodopsin dramatically exacerbates airway hyperreactivity of inflamed airways. Notably, these cells express the sphingosine-1-phosphate receptor 3 (S1PR3), and stimulation with a S1PR3 agonist efficiently induced broncho-constrictions, even in the absence of ovalbumin sensitization and inflammation. Our results show that the airway hyperreactivity phenotype can be physiologically dissociated from the immune component, and provide a platform for devising therapeutic approaches to asthma that target these pathways separately.

bronchospasms | airway inflammation

Asthma is an inflammatory disease of the airways causing about 250,000 deaths per year worldwide (1). Asthmatics suffer from pulmonary obstruction caused primarily by a decrease in the inner airway diameter as a result of excess mucus secretion and thickening of the walls of airways. In addition, asthmatic airways are hyperreactive to broncho-constricting stimuli. Thus, asthmatics frequently experience "asthma attacks," acute bronchospasms that severely obstruct breathing by further decreasing airway diameter (1–3). Notably, many asthma-related fatalities occur during the acute asthma attacks (4), a fact that emphasizes the urgent need for additional strategies to minimize broncho-constrictions in asthmatic airways.

Asthma can be induced by inhaled allergens like pollen or dust-mite excretes, or by viral infections (1, 5); these in turn trigger innate and adaptive immune responses involving multiple types of immune cells and inflammatory proteins (5). Genetic studies for loci linked to susceptibility to asthma have identified candidates involved in immune function (e.g., innate immunity, immunoregulation, and T-cell differentiation), epithelial cell function (e.g., genes involved in epithelial biology and mucosal immunity), and genes involved in lung function and the remodeling of airways (6). Although it is well established that the development of asthma and asthmatic symptoms are dependent on an immune response, suppressing immune responses and anti-inflammatory treatments only partially control symptoms, suggesting that cellular mechanisms outside the immune system add to the expression of this lung disease (3, 7, 8). Notably, a significant body of physiological data suggests that asthmatic symptoms may be significantly modulated by the nervous system (9, 10). Indeed, basic respiratory responses, such as cough, are mediated by sensory neurons innervating the lungs (11, 12). Furthermore, in addition to detecting and relaying the presence of nociceptive stimuli to brain centers, activated lung sensory neurons can themselves directly release proinflammatory peptides into surrounding tissue (13). Therefore, it is likely that these cells play an important modulatory role in lung inflammation (9, 14, 15).

Here we take a genetic approach to examine the contributions of molecularly defined populations of lung sensory neurons to hyperresponsive airways using a murine model of asthma. We show that a population of vagal sensory neurons, characterized by the expression of transient receptor potential vanilloid 1 (TRPV1) ion-channel, mediate airway hyperreactivity. We demonstrate that ablation of these cells abolishes the hyperreactive broncho-constrictions, even in the presence of a full lung inflammatory response, whereas their pharmacological or optogenetic activation dramatically exacerbates allergic airway hyperreactivity.

Results

Sensory Neurons Are Required for Allergic Airway Hyperreactivity. Neurons that innervate the lung are optimally positioned to sense chemical insults, as well as respond to bioactive molecules released during inflammation (10, 16–18). The cell bodies of these neurons reside in the vagal and cervical dorsal root ganglia (DRG) (19, 20), and signals from these cells are transmitted to the brainstem and the spinal cord to trigger pain and protective reflexes, respectively [e.g., cough (11)].

To investigate the contribution of lung sensory neurons to asthmatic symptoms, we used a murine ovalbumin model of allergic asthma (21). Our strategy was to ablate selective populations of neurons and examine its impact on asthma-like

Significance

Asthma is an inflammatory airway disease characterized by acute attacks in which airway constriction impedes breathing. The variable success of anti-inflammatory treatments in managing asthma attacks suggests that additional mechanisms contribute to this symptom. Here, we used a mouse model of acute asthma to show that a subset of sensory neurons mediates the hyperreactive airway responses. These findings define a cellular substrate outside the immune system that may serve as an important target in the management of asthmatic airway hyperreactivity.

Author contributions: D.T., M.A.H., and C.Z. designed research; D.T., N.H., K.S., and M.A.H. performed research; K.S. helped with RNAseq data; and D.T., M.A.H., and C.Z. wrote the paper.

Reviewer: D.L., New York University School of Medicine.

The authors declare no conflict of interest.

[1]To whom correspondence should be addressed. Email: cz2195@columbia.edu.

This article contains supporting information online at www.pnas.org/lookup/suppl/doi:10.1073/pnas.1411032111/-/DCSupplemental.

symptoms and responses. To induce an immune response in the lung and produce airway reactivity, mice were injected with ovalbumin for 3 wk, followed by 3 consecutive days of direct airway ovalbumin challenge (Fig. 1*A*) (22). Wild-type mice treated this way develop a robust immune reaction with increased serum levels of ovalbumin-specific IgE (Fig. 1*B*, *Left*) and lung infiltration of macrophages, eosinophilic, neutrophilic, and basophilic leukocytes (Fig. 1*B*, *Center* and *Right*). In addition, ovalbumin-sensitization leads to severe airway hyperreactivity, readily detected (i.e., as an increase in airway resistance) following acetylcholine-induced smooth-muscle contractions (Fig. 1 *C* and *F*).

To genetically ablate selective populations of sensory neurons, we relied on cre-dependent expression of diphtheria toxin (DTX) (23). Fig. 1 and Fig. S1 show that when TRPV1, TRPA1, and MrgD neurons are simultaneously ablated (TRP-DTA) [see *Materials and Methods* for details (24)], the resulting animals do not develop ovalbumin-dependent airway hyperreactivity (Fig. 1 *D* and *F*). However, these animals still display a fully developed immune reaction, including the production of allergen-specific immunoglobulins and leukocyte accumulation in the lungs (Fig. 1*B*). These results demonstrate that airway hyperreactivity, one of the most salient aspects of asthma, is dependent on sensory neurons. Furthermore, these data suggest that loss of a unique population of neurons may effectively dissociate the inflammatory component of the disease from the respiratory response.

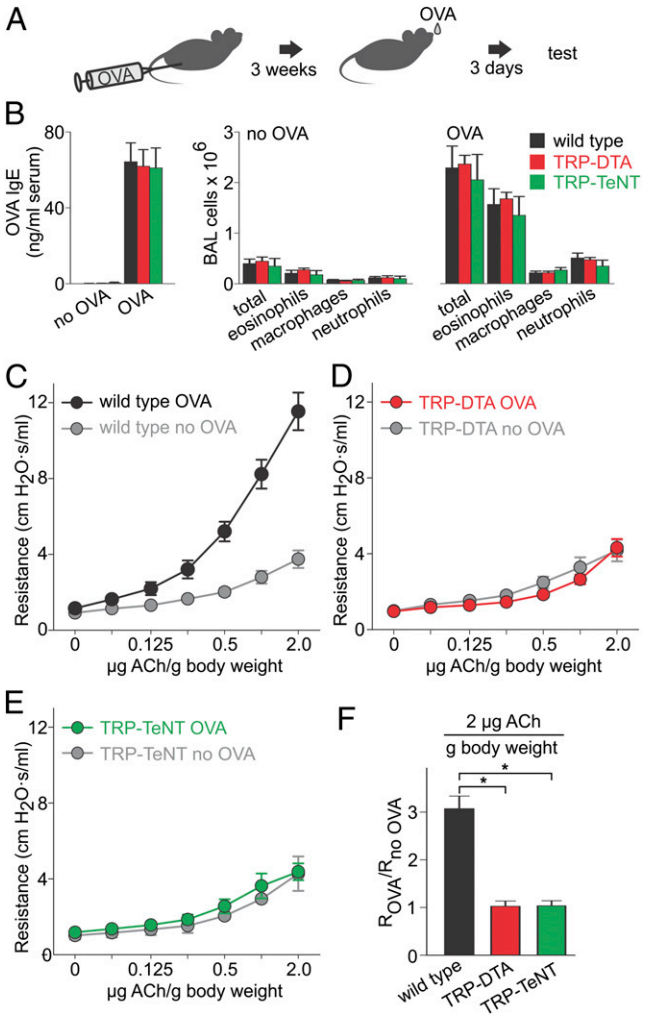

Fig. 1. Genetic ablation or silencing of sensory neurons abolishes asthma-like airway hyperreactivity. (*A*) Schematic of the standard ovalbumin-sensitized mouse model for acute asthma (21). (*B*) The levels of ovalbumin (OVA)-specific IgE (*Left*) and the numbers of immune cells in broncho-alveolar lavage (BAL) (*Center* and *Right*) are similar in control, TRP-DTA, and TRP-TeNT animals after OVA-sensitization ($n \geq 6$). (*C*) Airway resistance in response to acetylcholine stimulation (3, 22) in wild-type mice ($n \geq 10$). (*D*) Airway responses in TRP-DTA mice ($n \geq 5$), and (*E*) in TRP-TeNT mice ($n \geq 3$). (*F*) Ovalbumin induces a dramatic change of airway responses in wild-type, but not in TRP-DTA and TRP-TeNT mice (both *t* test $^*P < 0.001$). Data represent means ± SEM.

Allergic Airway Hyperreactivity Depends on Vesicle Release from Lung Sensory Neurons. Lung sensory neurons not only monitor, but are also likely to modulate the physiological state of the lungs (9, 10). Given our finding that TRP-expressing sensory neurons are required for the development of broncho-constrictions, we hypothesized that vesicle release from these neurons may be essential to produce this phenotype. Therefore, we engineered animals in which tetanus toxin light chain (TeNT) was genetically targeted to TRP-expressing cells (*Materials and Methods*) and then assayed their lung resistance in response to acetylcholine stimulation. Indeed, mice in which we functionally silenced TRP-expressing neurons by inactivating their synaptic and vesicle release/recycling machinery did not exhibit the expected inflammatory broncho-constriction phenotype (Fig. 1 *E* and *F*), even in the presence of a full lung inflammatory response (Fig. 1*B*).

Airway Hyperreactivity Is Abolished by Acute Ablation of TRPV1-Neurons in the Vagal Ganglion. The largest fraction of neurons genetically ablated and silenced in TRP-DTA and TRP-TeNT mice are defined by the expression of the TRPV1 ion channel (Fig. S1). Therefore, we set out to test whether the specific loss of TRPV1-cells could account for the loss of the airway hyperreactivity in these animals. To avoid potential side effects resulting from the loss of sensory neurons during development, we acutely ablated TRPV1-cells in adult animals. In essence, we targeted expression of the DTX receptor (DTR) (25) to TRPV1-cells (TRPV1-DTR) (26) (Fig. 2*A*) and coupled it with intraperitoneal injections of DTX at a time long after sensory neurons developed but before allergen sensitization with ovalbumin. Under this regime, the injected DTX will only be recognized and internalized by DTR-expressing cells, and only TRPV1-expressing cells will be ablated. We performed this experiment in 6- to 8-wk-old animals and confirmed the selective loss of TRPV1-neurons both in vagal ganglia and DRG by in situ hybridization (ISH) (Fig. 2*A* and Fig. S2) (26). Our results prove that selective ablation of TRPV1-expressing neurons is sufficient to prevent hyperreactive airway responses (Fig. 2*B*). This phenotype is highly specific as the loss of another major class of sensory neurons in vagal ganglia and DRG (e.g., MrgD-expressing neurons) has no impact on the hyperreactive airway response of ovalbumin-sensitized animals (Fig. 2*C*). Notably, the development of airway hyperreactivity is not dependent on the ion-channel TRPV1 itself (i.e., it requires the cells marked by the TRPV1 channel rather than the TRPV1 channel) (Fig. S3) (22). Interestingly, a loss-of-function mutation in TRPA1, a different member of the TRP family, reduces inflammatory airway hyperreactivity (22). However, in contrast to animals where we ablated TRPV1-expressing cells, TRPA1 knockouts also showed a profound deficit in their airway immune response (22), suggesting a different site or mode of action.

Next, we set out to identify the exact anatomical location of the TRPV1-expressing neurons required for airway hypersensitivity. The vagal ganglion provides the major source of lung sensory innervation (19, 20). Thus, we reasoned it may house the critical population of TRPV1-expressing neurons. Our approach was to acutely inject DTX directly into the vagal ganglia

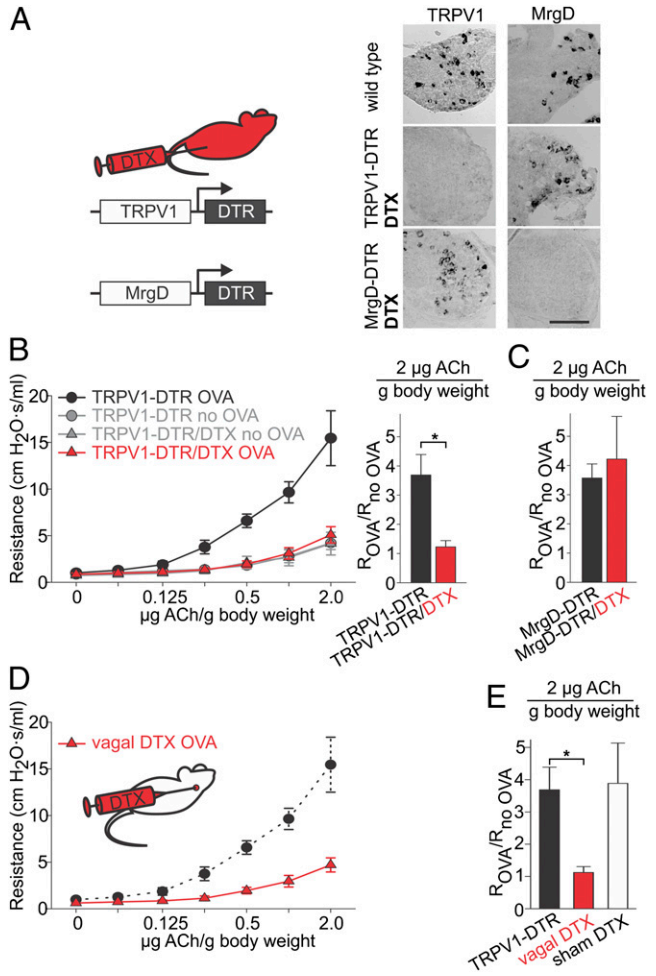

Fig. 2. Vagal TRPV1-expressing sensory neurons mediate allergic airway hyperreactivity. (*A*) Selective ablation of sensory neurons is achieved by injecting TRPV1-DTR or MrgD-DTR mice with DTX. TRPV1-DTR mice treated with DTX lose TRPV1-cells, but retain MrgD-expressing cells. Conversely, DTX treated MrgD-DTR mice lose MrgD-expressing cells, but retain TRPV1-cells. (Scale bar: 100 µm.) (*B*) Airway resistance in response to acetylcholine in TRPV1-DTR control mice ($n \geq 3$) and in animals challenged with DTX (TRPV1-DTR/DTX; $n = 6$). Ovalbumin changes airway responses in TRPV1-DTR but not in TRPV1-DTR/DTX mice (*t* test $^*P = 0.003$). (*C*) DTX-treated MrgD-DTR mice exhibit normal ovalbumin induced airway hyperreactivity ($n \geq 3$). (*D*) Airway resistance in response to acetylcholine in TRPV1-DTR mice challenged with direct vagal DTX injections ($n = 3$). The control responses shown as dashed lines (no DTX injection) are taken from *B* for comparison purposes. (*E*) Quantification of airway responses in vagal and sham DTX injections (i.e., DTX injections just outside the vagal ganglia, $n = 4$). Data represent means ± SEM; *t* test $^*P = 0.02$.

(bilaterally) of TRPV1-DTR mice. We hypothesized that this treatment would restrict the ablation of TRPV1-neurons only to the vagal ganglia and leave TRPV1-cells in the DRG (and other sites) intact. As predicted, there was a dramatic loss of TRPV1$^+$ cells in the vagal ganglia, whereas the number of TRPV1-neurons in the DRG were unaffected (Fig. S4). Importantly, loss of TRPV1-neurons in the vagal ganglia alone completely prevented the development of the inflammatory broncho-constriction phenotype (Fig. 2*D*). Control DTX injections just outside the vagal ganglia of TRPV1-DTR mice (Fig. 2*E*), or DTX injections into the vagal ganglia of DTR$^-$ control mice had no effect on airway hyperreactivity (Fig. S4). Taken together, these results substantiate the critical role of vagal TRPV1-cells in allergic airway hyperreactivity.

Vagal Sensory Neurons Modulate Airway Hyperreactivity. Given that the activity of vagal TRPV1-cells is necessary for the development of hyperreactive broncho-constrictions, we reasoned that direct stimulation of these sensory neurons may enhance the phenotype. We tested this postulate using two different strategies: Fig. 3 shows that vagal injections of capsaicin, a selective agonist of TRPV1, dramatically potentiated airway responses in allergic lungs (Fig. 3*A*, *Left*, and Fig. S5). However, capsaicin treatment had no effect on nonsensitized animals (Fig. 3*A*, *Right*). Next, we examined whether optogenetic activation of this population of neurons enhances the asthma-like broncho-constrictions. Therefore, we engineered mice that express the light-activatable channelrhodopsin (ChR2) ion channel in TRP-expressing

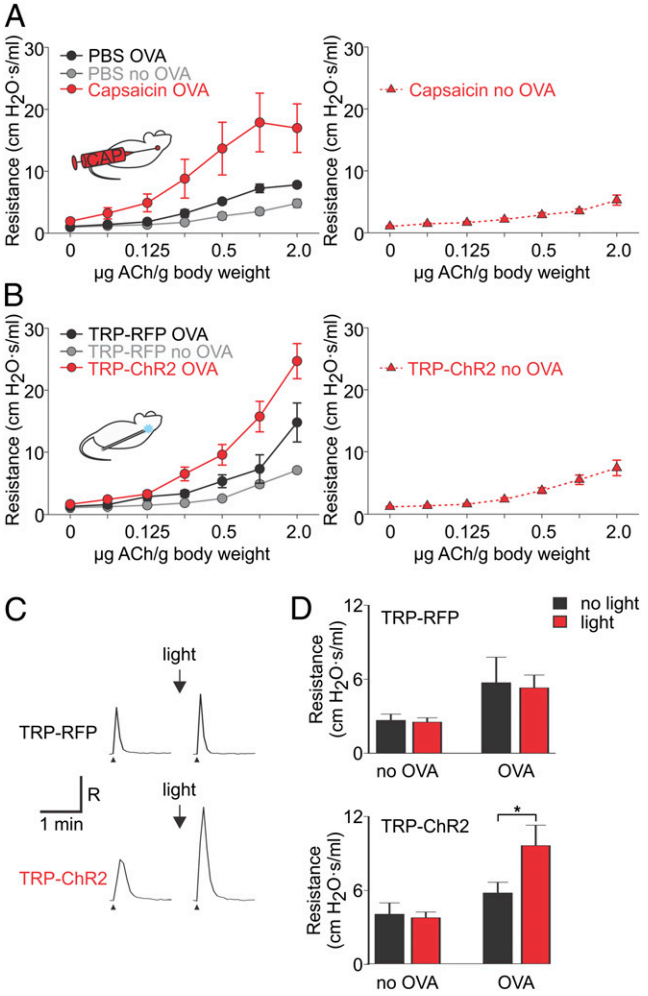

Fig. 3. Activation of vagal TRPV1-cells exacerbates allergic airway hyperreactivity. (*A*) Airway resistance in response to acetylcholine in C57BL/6 mice 1 h after vagal injection of PBS ($n \geq 5$) and 300 µM capsaicin ($n \geq 4$). (*B*) Airway resistance in response to acetylcholine in TRP-RFP and TRP-ChR2 mice ($n \geq 5$) after 1 h of vagal light stimulation. Note that stimulation of lung sensory neurons using optogenetics (or capsaicin, see *A*) has no effect on the baseline airway resistance in the absence of acetylcholine injections. (*C*) Recordings of airway resistance before and after light stimulation in an ovalbumin-sensitized TRP-RFP (*Upper*) and TRP-ChR2 (*Lower*) animal; small arrowhead indicates the time of acetylcholine injection (0.5 µg/g body weight). $R = 3$ cm H_2O·s/mL (*D*) Quantification of ChR2 responses. Vagal light stimulation increases the airway response in ovalbumin-sensitized TRP-ChR2 ($n = 7$; *t* test $^*P = 0.04$). In contrast, light has no effect on nonsensitized TRP-ChR2 or ovalbumin sensitized TRP-RFP control mice ($n = 5$). Data were obtained with 0.5 µg acetylcholine per gram body weight. Data represent means ± SEM.

sensory neurons (TRP-ChR2 mice), and used light guides to selectively illuminate the vagal ganglia (see *Materials and Methods* for details). Indeed, our results demonstrate that optogenetic activation caused a remarkable increase of the reactivity of immune-sensitized airways, but as expected, had no effect on healthy airways (Fig. 3 *B–D*).

Vagal Sensory Neurons Can Mediate Airway Hyperreactivity in the Absence of Inflammation. What are the signals that induce airway hyperreactivity in the asthmatic lung? Given that the effect of electric stimulation (i.e., ChR2) of vagal TRPV1-neurons still requires immune-sensitized airways, we hypothesized that the inflammatory cocktail produced during sensitization to ovalbumin challenges must contain specific bioactive molecules necessary to orchestrate the hyperreactive response, including perhaps the activation of additional signaling pathways in TRPV1-neurons. A prediction of this postulate is that direct exposure of such candidate signaling molecules to the vagal neurons might trigger the full airway hyperreactivity response, even in the absence of immune sensitization. Therefore, we searched for candidate receptors expressed in TRPV1 sensory neurons that could be activated by the inflammatory mixture. To this end we collected vagal TRPV1-neurons from TRPV1-reporter (TRPV1-eGFP) mice (27), and generated and sequenced representative cDNA-libraries from these cells. Bioinformatic analysis of the vagal TRPV1-cell transcriptome revealed a number of abundantly expressed candidate-receptor transcripts (Table S1). We focused our attention on the receptor for sphingosine-1-phosphate (S1PR3), for three reasons: (*i*) its expression is restricted to TRPV1$^+$ cells in the vagal ganglion (Fig. 4*A*); (*ii*) S1P levels are dramatically increased in ovalbumin-sensitized lungs of mice (Fig. S6); and (*iii*) S1PR3 has been broadly implicated as a potential player in the development of asthma in humans and in rodent models of the disease (28–30). To assess the effect of S1PR3 activation on airway responses, we used a S1PR3 agonist (FTY720) (31) and tested airway mechanics. Indeed, intravenous injection of FTY720 triggers robust airway hyperreactivity in the absence of immune sensitization with ovalbumin (Fig. 4 *B* and *C*) (31), but this response is totally absent in mice lacking sensory neurons (TRP-DTA) (Fig. 4*C*). Moreover, as would be predicted if S1PR-mediated pathways worked in concert with electrical activation of vagal sensory neurons during the course of an asthmatic response, the FTY720 responses to acetylcholine were also dramatically enhanced by optogenetic activation of the TRPV1-expressing neuron in vagal ganglia (Fig. 4*C*). Together, these results point to S1P as one of the signals that may be linking immune cell activity to the sensory neuron-dependent airway hyperreactivity in asthmatic responses.

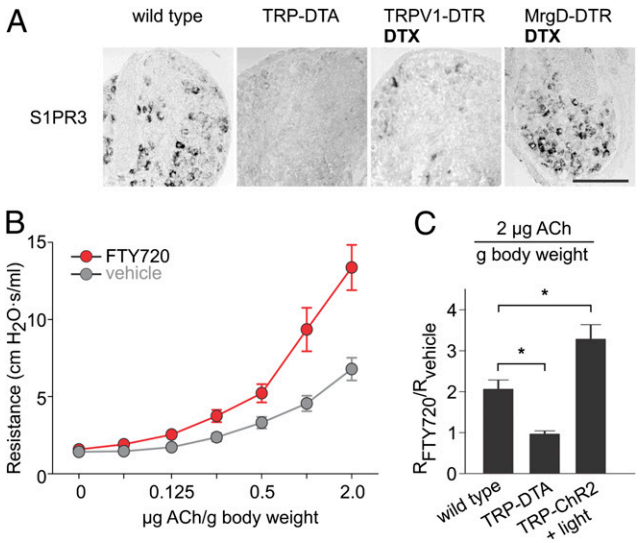

Fig. 4. S1P receptor activation induces airway hyperreactivity. (*A*) ISH experiments demonstrate that vagal neurons expressing S1PR3 are ablated in TRP-DTA and DTX-treated TRPV1-DTR mice, but not in control DTX-treated MrgD-DTR mice. (Scale bar: 100 µm.) (*B*) The S1PR3 agonist FTY720 (see *Materials and Methods* for dose and route of treatment) induces strong airway hyperreactivity in the absence of ovalbumen sensitization ($n \geq 4$; *t* test $P < 0.001$). (*C*) The effect of FTY720 on airway responses is abolished in animals without sensory neurons (TRP-DTA, $n = 3$; *t* test $^*P = 0.010$) and enhanced in mice with optogenetically activated vagal sensory neurons (TRP-ChR2, $n = 4$; *t* test $^*P = 0.003$). Data represent means ± SEM.

Concluding Remarks

Although much is known about the role of the immune system in the development of asthma and asthmatic symptoms, very little is known about the contribution of the peripheral nervous system to this disease. Here we took a molecular genetic approach to dissect the role of lung sensory neurons in a murine model of allergic airway inflammation (asthma-like), and identified vagal TRPV1-expressing neurons as essential players in the hyperreactive airway responses (see also ref. 22). We showed that the hyperreactivity phenotype of sensitized lungs can be physiologically dissociated from the immune component, and demonstrated how TRPV1 vagal sensory neurons can dramatically affect airway hyperreactivity, covering the full spectrum of phenotypes: from a total loss of hyperreactivity in animals lacking (or with synaptically silenced) TRPV1-neurons, to greatly exacerbating asthmatic-like broncho-constrictions in sensitized lungs via their direct optogenetic control, to triggering intense "de-novo" broncho-constrictions, even in the absence of an immune response following S1PR stimulation.

Taken together, our data support a model in which lung inflammation leads to the release of proinflammatory mediators that "sensitize" vagal sensory neurons (and their processes). These, in turn, modulate airway responses to broncho-constricting stimuli by acting like cellular "rheostats," thus translating the degree of inflammation into severity of airway hyperreactivity. The genetic dissociation of the airway hyperreactivity from the immunological components of inflamed lungs provides a noteworthy avenue for exploring therapies that may target TRPV1-expressing neurons as a strategy for the management of asthma attacks.

Materials and Methods

Chemicals. All chemicals were obtained from Sigma-Aldrich, unless otherwise stated.

Animals. TRPV1-Cre (24), ROSA-stop-RFP (32), ROSA-stop-ChR2 (32), ROSA-stop-DTA (23), ROSA-stop-TeNT (33), TRPV1-DTR (26), TRPV1-eGFP (27), MrgD-DTR (34), and TRPV1 knockout mice (35) have been described previously. ROSA-stop-RFP, ROSA-stop-ChR2, ROSA-stop-DTA, and C57BL/6 were purchased from Jackson Laboratories and were backcrossed to C57BL/6. TRPV1-eGFP mice were obtained from the Mutant Mouse Regional Resource Center. TRPV1-Cre animals were crossed to ROSA-stop-RFP, ROSA-stop-DTA, ROSA-stop-TeNT, or ROSA-stop-ChR2 mice to generate TRP-RFP, TRP-DTA, TRP-TeNT, and TRP-ChR2 animals, respectively. Experimental procedures were approved by the Institutional Animal Care and Use Committees at the Janelia Farm Research Campus. Animals were housed on a 12-h light-dark cycle with ad libitum access to water and food. All airway resistance, serum IgE, and immune cell infiltration experiments were measured in 10- to 16-wk-old female mice; DTX-treated animals were 14–22 wk at the time of testing. We note that the TRPV1-Cre animals also function as lineage tracers and may express the cre-dependent reporter in adult neurons that are no longer actively expressing TRPV1 (24). This potential difficulty was circumvented by carrying out acute ablations in adult animals via targeted expression of the DTR (26).

Sensitization and Airway Challenge Procedure. Mice were sensitized on days 0, 7, and 14 by intraperitoneal injection of 50 µg ovalbumin adsorbed in 2-mg

alum gel in a total volume of 200 μL PBS, as described previously (22). Control animals received alum gel only (no ovalbumin). Lightly anesthetized mice (isoflurane) were intranasally challenged with 50 μL 1% (wt/vol) ovalbumin in PBS or given PBS alone on days 21, 22, and 23. Airway-resistance measurements and sample collection were performed 24 h after the final intranasal challenge.

IgE Elisa and Cell Count Procedure. Ovalbumin-specific IgE concentrations in peripheral blood serum were determined in an ELISA using ovalbumin-coated 96-well plates and a biotinylated anti–mouse-IgE antibody. Ovalbumin-bound antibody complexes were detected colorimetrically using streptavidin-coupled HRP and TMB substrate. Antibodies, HRP, and TMB substrate were purchased from BD Bioscience. For leukocyte counts, cells were extracted from lungs in a broncho-alveolar lavage (22), concentrated using gentle centrifugation (200 × *g*, 10 min) and suspended in 0.1 mL PBS. Ten microliters of the cell suspension were placed on a microscope slide, and counted after Wright-Giemsa staining (HEMA-3 Stain, Fisher Scientific). Cell counts were used to estimate total cell numbers present in each lavage.

Measurement of Airway Reactivity. Mice were anesthetized with Ketamine (100 mg/kg) and Xylazine (10 mg/kg), and paralyzed with Vecuronium Bromide (Bedford Laboratories; 0.02 mg/kg i.p.). For measurement of airway resistance, animals were connected to a Flexivent pulmonary mechanics analyzer (SCIREQ) via a tracheal cannula (22). Lung tidal volume and breathing rates were set at of 9 mL/kg and 150 bpm, respectively (positive end-expiratory pressure was set at 3 cm H_2O). Acetylcholine (0.06, 0.125, 0.25, 0.5, 1.0, and 2.0 μg/kg) was administer through the jugular vein to generate the concentration-response curves of airway resistance. Measurements of airway mechanics were made continuously applying the single-compartment model (36). Further details of the protocol can be found at http://or.ucsf.edu/rrp/14893-DSY.html.

DTX-Mediated Cell Ablation. For systemic DTX-mediated cell ablation, 200 ng DTX in PBS was injected intraperitoneally once a day over 3 wk. For vagal delivery of DTX, mice were first intubated under isoflurane anesthesia for mechanical ventilation during the vagal injection procedure; this was necessary because mice frequently experienced respiratory arrest after manipulations of the right vagus nerve. For intubation, vocal cords were treated with 4% (wt/vol) Lidocaine gel (Fougera), followed by placement of a 20-gauge catheter (BD Insyte Autoguard) into the trachea between larynx and carina. A mechanical respirator (FlexiVent) delivered 1–2% (vol/vol) isoflurane in oxygen at a tidal volume and a respiration frequency optimized for the animal's weight (0.14–0.20 mL, 140–170 cycles per minute). A lateral skin incision (1 cm) was made in the neck with the animal in a supine position, and the vagal ganglia exposed by retracting the digastric muscle. PBS containing 20 ng DTX (200-nL total volume) and 5% (vol/vol) RetroBeads (for confirming the site of injection; Lumafluor) were injected (over 3–5 min) either bilaterally into the caudal end (vagal DTX) or in the vicinity of the exposed vagal ganglion (sham DTX) using 20-μm tip-diameter glass micropipettes.

Optogenetic and Pharmacological Stimulation of Vagal Sensory Neurons. Optic fibers (400-μm core branching fiberoptic patchcord; Doric Lenses) were placed bilaterally about 2 mm above the caudal end of the vagal ganglion. Stimulation was by means of a 470-nm light source (Connectorized High Brightness LED, Doric Lenses); the standard protocol used 25-ms pulses at 10 Hz, intensity: 60–100 mW/mm^2. For pharmacological stimulation with capsaicin, exposed vagal ganglia were injected (over 3–5 min) bilaterally with 200 nL of 300 μM capsaicin in PBS and 5% (vol/vol) RetroBeads (Lumafluor) or PBS with RetroBeads alone (control) 1 h before airway measurements. Injections were performed using beveled glass micropipettes (20-μm tip diameter) and a microinjector (MO-10; Narishige). For pharmacological stimulation with FTY720 (Selleck Chem; 1 mg/kg), the compound was diluted in ethanol and injected into the jugular vein 1 h before airway measurements. Control animals were injected with vehicle only.

In Situ Hybridization. ISH and double-label ISH were performed at high stringency (washed 30 min, 0.2 × SSC, 70 °C) as described previously (20). For double-label ISH, we used fluorescein- and digoxigenin-labeled probes as described previously (24). Images were collected using a Microphot FX microscope (Nikon) or a Leica TCS SP2 (Leica Microsystems) confocal microscope. Images were processed with CorelDraw.

Cell Profiling. Cells were sorted as previously described (37). Isolated ganglia were digested in 1 mg/mL pronase for 1 h and then triturated with Pasteur pipettes of decreasing tip diameter; dissociated cells were then picked manually with a glass pipette (tip diameter, 50 μm). Total RNA was extracted from 30~100 labeled cells (Picopure kit; Invitrogen) and amplified using the Ovation RNASeq v2 kit (NuGEN). Libraries were sequenced using an Illumina HiSEq. 2500 (single-end 95-bp reads).

ACKNOWLEDGMENTS. We thank the Sandler Asthma Basic Research Center core facility at the University of California at San Francisco and Xiaozhu Huang for help (and training) with the asthma murine model; Jim Cox and Michael Flynn of Janelia Farm's animal services for help, advice, and support; Iwona Stepniak, Amanda Wardlaw, Miriam Rose, Emily Bowman, and Lihua Wang for expert technical support; Megan Williams, Loren Looger, and Matthew Hockin for helpful comments; and David Anderson and Martyn Goulding for their generous gifts of MrgD-DTR and Rosa-TeNT mice, respectively. The mouse stock Tg(TRPV1-EGFP) was obtained from the Mutant Mouse Regional Resource Center, a National Center for Research Resources, National Institutes of Health-funded strain repository, and was donated to the Mutant Mouse Regional Resource Center by the National Institute of Neurological Disorders and Stroke-funded Gene Expression Nervous System Atlas Bacterial Artificial Chromosome transgenic project. This manuscript resulted from Grant 09-0257 from the American Asthma Foundation (to C.Z.), and was supported in part by the National Institute of Dental and Craniofacial Research (M.A.H.). C.Z. is an Investigator of the Howard Hughes Medical Institute and a Senior Fellow at the Janelia Farm Research Campus, Howard Hughes Medical Institute.

1. Anonymous (2014) *Global Strategy for Asthma Management and Prevention*. Global Initiative for Asthma (GINA) 2014. Available at: http://www.ginasthma.org/.
2. Program NAEaP (2007) *Expert Panel Report 3: Guidelines for the Diagnosis and Management of Asthma* (National Institutes of Health, Bethesda, MD), p 440.
3. Katsumoto TR, et al. (2013) The phosphatase CD148 promotes airway hyperresponsiveness through SRC family kinases. *J Clin Invest* 123(5):2037–2048.
4. McFadden ER, Jr., Warren EL (1997) Observations on asthma mortality. *Ann Intern Med* 127(2):142–147.
5. Locksley RM (2010) Asthma and allergic inflammation. *Cell* 140(6):777–783.
6. Vercelli D (2008) Discovering susceptibility genes for asthma and allergy. *Nat Rev Immunol* 8(3):169–182.
7. Reddy D, Little FF (2013) Glucocorticoid-resistant asthma: More than meets the eye. *J Asthma* 50(10):1036–1044.
8. Gu X, et al. (2014) Chemosensory functions for pulmonary neuroendocrine cells. *Am J Respir Cell Mol Biol* 50(3):637–646.
9. Barnes PJ (1986) Asthma as an axon reflex. *Lancet* 1(8475):242–245.
10. Undem BJ, Carr MJ (2002) The role of nerves in asthma. *Curr Allergy Asthma Rep* 2(2): 159–165.
11. Geppetti P, Patacchini R, Nassini R, Materazzi S (2010) Cough: The emerging role of the TRPA1 channel. *Lung* 188(Suppl 1):S63–S68.
12. Bessac BF, Jordt SE (2008) Breathtaking TRP channels: TRPA1 and TRPV1 in airway chemosensation and reflex control. *Physiology (Bethesda)* 23:360–370.
13. Hökfelt T, Kellerth JO, Nilsson G, Pernow B (1975) Experimental immunohistochemical studies on the localization and distribution of substance P in cat primary sensory neurons. *Brain Res* 100(2):235–252.
14. Adriaensen D, Timmermans JP (2011) Breath-taking complexity of vagal C-fibre nociceptors: Implications for inflammatory pulmonary disease, dyspnoea and cough. *J Physiol* 589(Pt 1):3–4.
15. Richardson JD, Vasko MR (2002) Cellular mechanisms of neurogenic inflammation. *J Pharmacol Exp Ther* 302(3):839–845.
16. Chiu IM, et al. (2013) Bacteria activate sensory neurons that modulate pain and inflammation. *Nature* 501(7465):52–57.
17. Coleridge HM, et al. (1976) Stimulation of 'irritant' receptors and afferent C-fibres in the lungs by prostaglandins. *Nature* 264(5585):451–453.
18. Bautista DM, et al. (2006) TRPA1 mediates the inflammatory actions of environmental irritants and proalgesic agents. *Cell* 124(6):1269–1282.
19. Springall DR, et al. (1987) Retrograde tracing shows that CGRP-immunoreactive nerves of rat trachea and lung originate from vagal and dorsal root ganglia. *J Auton Nerv Syst* 20(2):155–166.
20. Kummer W, Fischer A, Kurkowski R, Heym C (1992) The sensory and sympathetic innervation of guinea-pig lung and trachea as studied by retrograde neuronal tracing and double-labelling immunohistochemistry. *Neuroscience* 49(3):715–737.
21. Nials AT, Uddin S (2008) Mouse models of allergic asthma: Acute and chronic allergen challenge. *Dis Model Mech* 1(4-5):213–220.
22. Caceres AI, et al. (2009) A sensory neuronal ion channel essential for airway inflammation and hyperreactivity in asthma. *Proc Natl Acad Sci USA* 106(22):9099–9104.
23. Ivanova A, et al. (2005) In vivo genetic ablation by Cre-mediated expression of diphtheria toxin fragment A. *Genesis* 43(3):129–135.
24. Mishra SK, Tisel SM, Orestes P, Bhangoo SK, Hoon MA (2011) TRPV1-lineage neurons are required for thermal sensation. *EMBO J* 30(3):582–593.

25. Saito M, et al. (2001) Diphtheria toxin receptor-mediated conditional and targeted cell ablation in transgenic mice. *Nat Biotechnol* 19(8):746–750.
26. Pogorzala LA, Mishra SK, Hoon MA (2013) The cellular code for mammalian thermosensation. *J Neurosci* 33(13):5533–5541.
27. Gong S, et al. (2003) A gene expression atlas of the central nervous system based on bacterial artificial chromosomes. *Nature* 425(6961):917–925.
28. Trifilieff A, Fozard JR (2012) Sphingosine-1-phosphate-induced airway hyperreactivity in rodents is mediated by the sphingosine-1-phosphate type 3 receptor. *J Pharmacol Exp Ther* 342(2):399–406.
29. Ammit AJ, et al. (2001) Sphingosine 1-phosphate modulates human airway smooth muscle cell functions that promote inflammation and airway remodeling in asthma. *FASEB* 15(7):1212–1214.
30. Trifilieff A, Baur F, Fozard JR (2009) Role of sphingosine-1-phosphate (S1P) and the S1P(2) receptor in allergen-induced, mast cell-dependent contraction of rat lung parenchymal strips. *Naunyn Schmiedebergs Arch Pharmacol* 380(4):303–309.
31. Brinkmann V, et al. (2002) The immune modulator FTY720 targets sphingosine 1-phosphate receptors. *J Biol Chem* 277(24):21453–21457.
32. Madisen L, et al. (2010) A robust and high-throughput Cre reporting and characterization system for the whole mouse brain. *Nat Neurosci* 13(1):133–140.
33. Zhang Y, et al. (2008) V3 spinal neurons establish a robust and balanced locomotor rhythm during walking. *Neuron* 60(1):84–96.
34. Cavanaugh DJ, et al. (2009) Distinct subsets of unmyelinated primary sensory fibers mediate behavioral responses to noxious thermal and mechanical stimuli. *Proc Natl Acad Sci USA* 106(22):9075–9080.
35. Caterina MJ, et al. (2000) Impaired nociception and pain sensation in mice lacking the capsaicin receptor. *Science* 288(5464):306–313.
36. Davis GM, Coates AL, Dalle D, Bureau MA (1988) Measurement of pulmonary mechanics in the newborn lamb: A comparison of three techniques. *J Appl Physiol (1985)* 64(3):972–981.
37. Hempel CM, Sugino K, Nelson SB (2007) A manual method for the purification of fluorescently labeled neurons from the mammalian brain. *Nat Protoc* 2(11):2924–2929.

Supporting Information

Tränkner et al. 10.1073/pnas.1411032111

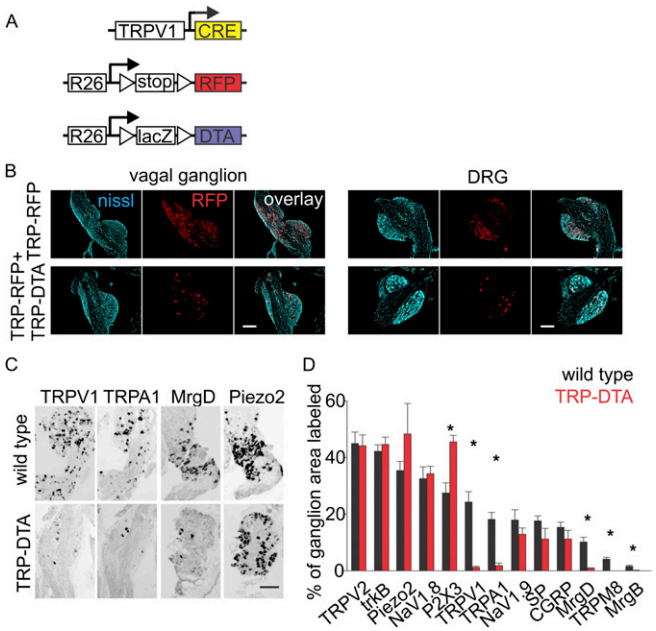

Fig. S1. Vagal ganglia in TRP-DTA animals. (*A*) Schematic of transgenes used for genetic labeling and ablation of sensory neurons. (*B*) In TRP-RFP mice, about half the cells in vagal ganglia (*Upper Left*) and the dorsal root ganglia (DRG) (*Upper Right*) express RFP. Most fluorescently labeled cells are ablated upon Cre-dependent expression of diphtheria toxin (DTA) (*Lower*). Nissl-stain: NeuroTrace (Molecular Probes). (*C*) Vagal ganglia of TRP-DTA mice lose TRPV1, TRPA1, and MrgD-expressing sensory neurons, but retain mechanoreceptors (marked by Piezo2). (*D*) Quantification of the relative abundances of the various cell populations in control and DTA-ablated animals; each marker was tested by in situ hybridizations in at least three different mice. TRPV2: transient receptor potential cation channel, subfamily V, member 2; trkB: neurotrophic tyrosine kinase, receptor, type 2; Piezo2: piezo-type mechanosensitive ion channel component 2; NaV1.8: sodium channel, voltage-gated, type X, α; P2X 3: purinergic receptor P2X, ligand-gated ion channel, 3; TRPV1: transient receptor potential cation channel, subfamily V, member 1; TRPA1: transient receptor potential cation channel, subfamily A, member 1; NaV1.9: sodium channel, voltage-gated, type XI, α; SP: substance P; CGRP: calcitonin/calcitonin-related polypeptide α and β; MrgD: MAS-related GPR, member D; TRPM8: transient receptor potential cation channel, subfamily M, member 8; MrgB: MAS-related GPR, member B subtypes; Data represent means ± SEM. Asterisks indicate statistically significant differences between wild-type and TRP-DTA animals (*t*-test **P* values): 0.002 (P2X3), 0.001 (TRPV1), <0.001 (TRPA1), 0.011 (MrgD), <0.001 (TRPM8), 0.006 (MrgB). (Scale bars: 100 μm.)

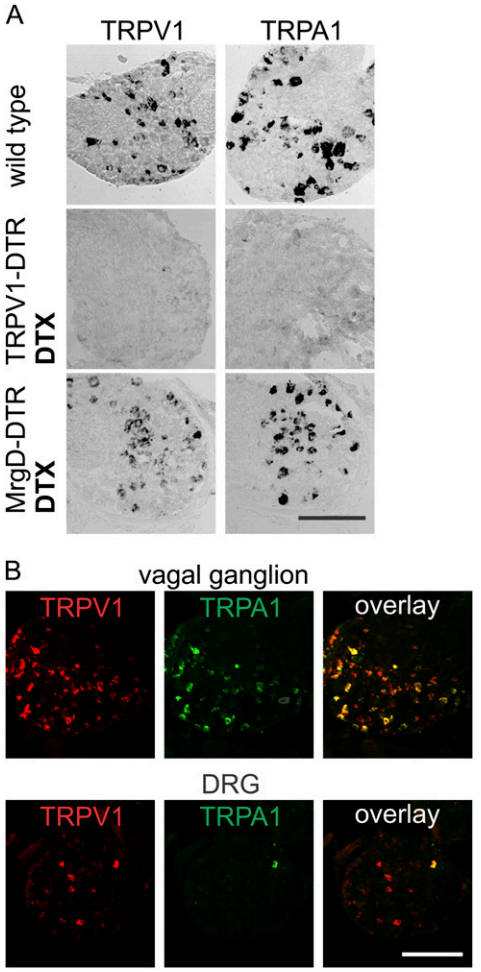

Fig. S2. Lung sensory neurons coexpress TRPV1 and TRPA1. (*A*) Diptheria toxin (DTX) treatment of TRPV1-DTR mice (but not MrgD-DTR mice) leads to the loss of TRPV1- and TRPA1-expressing cells. (*B*) Double-fluorescence in situ experiments demonstrate that most TRPV1 neurons also coexpress TRPA1 (*Upper*). In contrast, only a subset of DRG neurons coexpress TRPV1 and TRPA1. (Scale bars: 100 μm.)

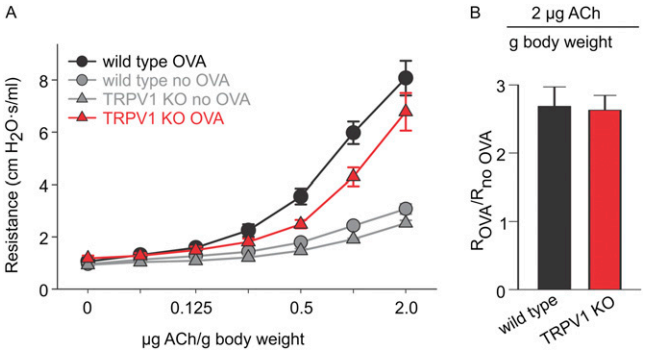

Fig. S3. Allergic airway hyperreactivity in TRPV1 knockout mice. (*A*) Airway resistance in response to acetylcholine in TRPV1 knockout (1) and wild-type littermates ($n \geq 5$). (*B*) Ovalbumin (OVA) induces a similar change in airway hyperreactivity in TRPV1 knockout and wild-type controls (see also ref. 2). Data represent means ± SEM; *t* test $P = 0.274$.

1. Caterina MJ, et al. (2000) Impaired nociception and pain sensation in mice lacking the capsaicin receptor. *Science* 288(5464):306–313.
2. Caceres AI, et al. (2009) A sensory neuronal ion channel essential for airway inflammation and hyperreactivity in asthma. *Proc Natl Acad Sci USA* 106(22):9099–9104.

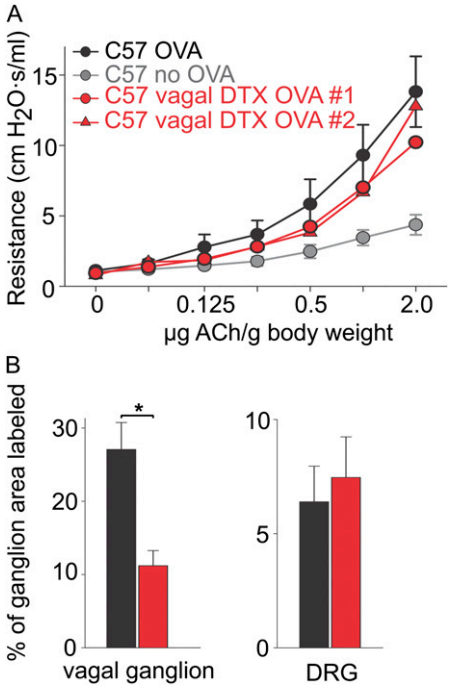

Fig. S4. DTX-injections. (*A*) Airway resistance in two control DTR$^-$ mice following vagal injection of DTX (untreated controls $n \geq 5$). DTX-injected and uninjected DTR$^-$ mice show similar hyperreactive airway responses (*t* test, $P = 0.64$). (*B*) Quantification of the relative abundance of TRPV1-cells in the vagal ganglia of TRPV1-DTR animals injected with DTX (red bars; $n = 3$); black bars show the relative abundance of TRPV1-cells in the vagal ganglia of control uninjected mice ($n \geq 3$); also shown as a control are TRPV1 quantifications in the DRG ganglion. As expected, there are no differences in the DRG of vagal-injected or uninjected animals. Data represent means ± SEM; *t* test, $^*P = 0.019$.

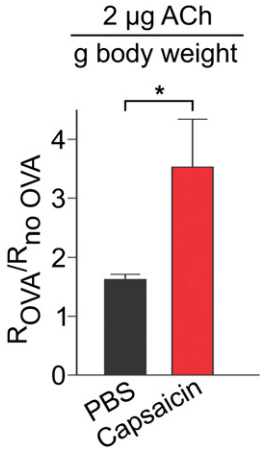

Fig. S5. Capsaicin activation of lung sensory neurons exacerbates allergic airway hyperreactivity. See main text for details. Shown is the quantification of the hyperreactive responses of ovalbumin-sensitized mice after stimulation of vagal TRPV1-cells with capsaicin ($n = 4$; *t* test, $^*P = 0.04$). Data represent means ± SEM.

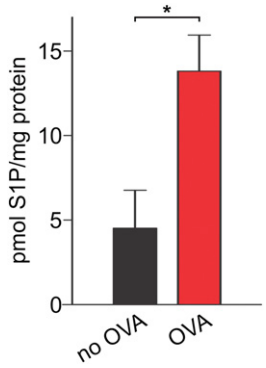

Fig. S6. Sphingosine-1-phosphate concentrations in lung tissue. The levels of the endogenous S1PR3 ligand spingosine-1-phosphate (S1P), as measured by ELISAs (Echelon BioScience), significantly increase with ovalbumin sensitization (*t* test, $*P = 0.04$). Data represent means ± SEM.

Table S1. Receptors expressed in vagal TRPV1-cells

Symbol	FPKM sample #1	FPKM sample #2	FPKM sample #3	Mean	SD
Ngfr	584.3	401.1	428.3	471.2	98.9
F2r	382.3	251.5	373.2	335.7	73.0
Htr3a	276.2	284.0	253.6	271.3	15.8
Bcam	146.0	174.8	144.7	155.2	17.0
S1pr3	**119.0**	**168.4**	**167.6**	**151.6**	**28.3**
P2rx2	159.2	93.9	149.5	134.2	35.2
P2rx3	118.3	91.6	140.8	116.9	24.6
Oprm1	87.4	118.6	121.0	109.0	18.7
Gnb2l1	79.3	97.6	102.9	93.3	12.4
Cysltr2	69.5	43.9	147.6	87.0	54.0
Gabbr1	79.0	86.3	85.2	83.5	3.9
Ldlr	84.9	76.5	74.0	78.5	5.7
Il6st	54.1	102.9	70.2	75.8	24.9
Ret	57.2	82.1	67.1	68.8	12.6
Ntrk2	79.4	43.5	78.7	67.2	20.5
Rtn4rl1	70.7	46.5	78.5	65.2	16.7
Adipor1	66.0	66.4	63.1	65.2	1.8
Gfra3	7.2	172.2	10.6	63.3	94.3
Npy2r	64.2	52.2	61.7	59.4	6.3
Gabrb3	56.2	49.4	54.9	53.5	3.6
Lgals3bp	52.2	50.9	51.6	51.6	0.7
Htr3b	54.8	40.9	58.2	51.3	9.2
Gria4	50.7	35.2	58.4	48.1	11.8
Trpv1	37.0	60.1	46.7	47.9	11.6
Slc22a17	43.2	42.1	46.8	44.0	2.5
Lphn1	32.7	41.9	41.1	38.5	5.1
Cd44	13.4	71.1	25.1	36.5	30.5
Thra	27.0	37.0	43.0	35.7	8.1
Sigmar1	22.5	55.9	25.7	34.7	18.4
Neo1	36.8	27.0	37.0	33.6	5.7
Npy1r	4.4	90.4	4.5	33.1	49.6
Glp1r	47.1	15.7	31.2	31.3	15.7
Sv2a	30.9	24.2	35.6	30.3	5.7
Sema4d	25.4	29.3	33.8	29.5	4.2
Grin1	25.8	28.7	32.6	29.0	3.4
Sema5a	35.5	19.7	31.2	28.8	8.2
Cnr1	24.4	21.1	32.2	25.9	5.7
Il10rb	24.1	21.4	31.9	25.8	5.5
Crcp	23.8	22.8	29.0	25.2	3.3
Npr2	26.4	22.5	26.3	25.1	2.2
Crhr2	32.6	15.4	26.3	24.8	8.7
Cntfr	15.8	31.9	25.2	24.3	8.1
Tfrc	26.8	26.3	17.8	23.6	5.1
Paqr4	16.6	28.9	20.1	21.9	6.4
Fzd3	23.0	16.2	25.7	21.6	4.9
Unc5c	27.5	13.5	21.2	20.8	7.0
Ntrk1	14.5	41.2	6.2	20.6	18.3
Osmr	11.8	40.5	7.1	19.8	18.1
Paqr8	19.4	18.6	20.0	19.3	0.7
Paqr9	16.2	20.6	19.5	18.8	2.3
Inpp5k	19.2	18.4	17.3	18.3	1.0
Xpr1	18.2	20.7	15.6	18.2	2.6
Gpr56	9.5	30.7	13.9	18.0	11.2
Tm2d1	14.9	20.3	14.4	16.5	3.3
Igf1r	13.5	18.2	17.4	16.4	2.5
Atrn	14.2	15.3	17.4	15.6	1.6
Gria2	15.7	11.8	18.2	15.2	3.2
Abca7	14.8	14.8	15.3	15.0	0.3
Gpr35	11.3	17.7	14.4	14.5	3.2
Acvr1b	10.7	15.7	16.8	14.4	3.2
Gria3	18.1	5.2	18.4	13.9	7.6
Nrp2	17.3	8.4	15.8	13.8	4.7

Table S1. Cont.

Symbol	FPKM sample #1	FPKM sample #2	FPKM sample #3	Mean	SD
Ifnar2	15.3	13.4	12.1	13.6	1.6
Plxna4	6.1	25.6	7.4	13.0	10.9
Nlgn2	11.7	17.3	8.8	12.6	4.3
Paqr7	10.4	12.8	14.1	12.4	1.8
Adora2a	9.7	6.8	17.9	11.5	5.7
Drd2	14.4	8.6	9.9	11.0	3.0
Flt1	11.9	7.6	13.4	10.9	3.0
Ednra	13.6	6.0	13.0	10.9	4.2
Grin3a	10.5	11.3	10.6	10.8	0.5
Grm7	8.4	14.5	9.2	10.7	3.3
Nlgn3	11.0	11.9	9.2	10.7	1.4
P2rx4	10.6	10.7	10.4	10.6	0.1
Grik5	9.3	9.9	10.7	10.0	0.7
Ptger4	6.1	11.7	12.0	9.9	3.3
Med1	10.2	9.8	9.7	9.9	0.3
Med16	8.6	12.3	8.6	9.8	2.1
Tub	11.4	5.4	11.9	9.6	3.6
Gabrg2	8.7	9.2	10.3	9.4	0.8
Plxna2	6.5	15.5	5.4	9.1	5.6
Adipor2	8.7	8.9	9.7	9.1	0.5
Ifnar1	7.2	10.5	6.5	8.1	2.1
Arnt	6.6	11.2	6.3	8.0	2.7
Agtrap	5.7	12.0	6.4	8.0	3.5
Insr	8.2	7.7	7.8	7.9	0.3
Unc13c	7.7	7.2	8.7	7.9	0.8
Kit	1.7	17.0	4.3	7.7	8.2
Fcgrt	6.8	5.6	10.1	7.5	2.3
Fgfr1	7.8	8.2	6.0	7.3	1.1
Frzb	3.9	11.8	6.3	7.3	4.0
Gfra1	8.2	7.6	6.1	7.3	1.1
Sfrp1	8.6	4.9	7.9	7.2	2.0
Gpr173	6.3	6.6	8.7	7.2	1.3
Plxnd1	3.7	10.4	6.2	6.8	3.4
Nrp1	7.4	7.2	5.4	6.7	1.1
Htr1b	3.7	13.1	2.8	6.5	5.7
Lrp8	6.0	8.7	4.8	6.5	2.0
Plxna3	5.8	6.2	7.1	6.4	0.7
Rxrb	5.5	7.6	5.9	6.4	1.1
Ly96	5.6	9.9	3.0	6.1	3.5
Ptgdr	3.3	7.1	7.8	6.1	2.4
Siva1	6.0	4.6	7.1	5.9	1.2
Ddr1	5.0	7.2	5.5	5.9	1.1
Chrm4	6.5	5.0	6.0	5.8	0.8
Ghr	5.9	6.1	4.5	5.5	0.9
Lrp6	3.7	6.1	6.4	5.4	1.5
Nr3c1	3.3	9.2	2.9	5.1	3.5
Jmjd6	6.1	4.0	5.1	5.1	1.0
Htr5b	7.5	1.6	5.8	5.0	3.0
Tspan12	5.2	3.8	5.8	4.9	1.0
Gpr161	3.7	3.3	7.7	4.9	2.4
Htr5a	4.3	5.2	5.0	4.8	0.5
Ar	2.6	4.8	6.2	4.5	1.8
Acvr1	4.3	5.3	3.8	4.5	0.8
Pth1r	2.6	6.2	4.5	4.4	1.8
Ddr2	6.5	2.2	4.7	4.4	2.2
Epha5	3.3	4.7	5.2	4.4	1.0
Gfra4	3.3	3.2	6.6	4.3	1.9
Grik4	3.7	6.1	2.9	4.2	1.6
Agtr1a	4.5	1.2	6.8	4.2	2.8
Ednrb	2.0	6.5	3.7	4.1	2.3
Fzd5	4.9	3.1	4.2	4.1	0.9

Table S1. Cont.

Symbol	FPKM sample #1	FPKM sample #2	FPKM sample #3	Mean	SD
Itpr1	4.7	2.8	4.7	4.1	1.1
Ptk7	3.3	2.6	6.2	4.1	1.9
Unc13b	3.3	5.8	2.8	4.0	1.6
Tgfbr1	1.9	6.1	3.0	3.7	2.2
B9d1	4.1	3.4	3.1	3.5	0.5
Tnfrsf11a	2.4	4.6	3.2	3.4	1.1
Cckbr	2.3	3.5	4.4	3.4	1.0
Cd97	3.6	3.9	2.5	3.3	0.8
Ptch1	2.1	2.8	4.9	3.3	1.4
Il1r1	3.9	4.0	1.9	3.3	1.2
Hyal2	2.0	4.8	2.6	3.2	1.5
P2rx5	1.8	5.9	1.7	3.2	2.4
Ppard	1.5	2.6	5.1	3.1	1.9
Htr1a	0.5	8.0	0.3	2.9	4.4
Plxna1	2.5	2.4	3.6	2.8	0.7
Gria1	0.6	6.8	0.6	2.7	3.6
Pgr	2.9	2.4	2.6	2.6	0.2
Tnfrsf1a	2.4	3.4	2.0	2.6	0.7
Grik1	2.3	1.4	3.9	2.5	1.3
Kiss1r	2.9	1.8	2.9	2.5	0.6
Rxrg	1.8	4.4	1.1	2.4	1.8
Ryk	2.2	2.5	2.5	2.4	0.2
Rtn4rl2	2.0	3.7	1.4	2.4	1.2
Scarb1	2.1	3.9	1.0	2.3	1.5
Celsr1	2.3	2.9	1.8	2.3	0.5
Thrb	3.4	1.3	2.2	2.3	1.1
Ntsr2	0.3	5.6	0.8	2.2	2.9
Olfr920	2.6	1.4	2.5	2.1	0.7
Grik2	2.1	1.9	2.3	2.1	0.2
Plxnb2	2.0	2.2	2.0	2.1	0.1
Kdr	1.6	2.3	2.3	2.1	0.4
Lrp1b	1.8	2.0	2.4	2.0	0.3
Paqr3	1.4	3.2	1.5	2.0	1.0
Sfrp5	1.2	1.3	3.6	2.0	1.4
Lgr4	1.1	3.4	1.4	2.0	1.2

TRPV1-eGFP^{+} cells from the vagal ganglia were isolated, manually picked (*Materials and Methods*) and subjected to RNA-Seq (1). Sequenced fragments from three separately collected samples were mapped to the mouse genome (UCSC mm10) using STAR (2), and fragments per kilobase per million reads (FPKM) were calculated with Cufflinks using Illumina iGenome mm10 (3). The list includes receptor-transcripts present at ≥10 copies per cell based on spiked-in synthetic standards (≥2 FPKM) (4). Receptors were identified using gene ontology GO:0004872 (5) (with evidence code corresponding to manual annotation; www.ebi.ac.uk/QuickGO), and rank ordered according to mean FPKMs. Sample 1 is from a male, and samples 2–3 from female mice; mice were 41- to 43-wk-old at the time of tissue collection. *S1pr3* is highlighted in boldface.

1. Mortazavi A, Williams BA, McCue K, Schaeffer L, Wold B (2008) Mapping and quantifying mammalian transcriptomes by RNA-Seq. *Nat Methods* 5(7):621–628.
2. Dobin A, et al. (2013) STAR: Ultrafast universal RNA-seq aligner. *Bioinformatics* 29(1):15–21.
3. Trapnell C, et al. (2010) Transcript assembly and quantification by RNA-Seq reveals unannotated transcripts and isoform switching during cell differentiation. *Nat Biotechnol* 28(5):511–515.
4. Jiang L, et al. (2011) Synthetic spike-in standards for RNA-seq experiments. *Genome Res* 21(9):1543–1551.
5. Ashburner M, et al.; The Gene Ontology Consortium (2000) Gene ontology: Tool for the unification of biology. *Nat Genet* 25(1):25–29.